



Article

A 0.5 V, 32 nW Compact Inverter-Based All-Filtering Response Modes Gm-C Filter for Bio-Signal Processing

Ali Namdari *, Orazio Aiello and Daniele D. Caviglia

Department of Electrical, Electronic, Telecommunications Engineering and Naval Architecture (DITEN),
University of Genova, Via Opera Pia 11a, I-16145 Genoa, Italy; orazio.aiello@unige.it (O.A.)

* Correspondence: ali.namdari@edu.unige.it

Abstract: A low-power, low-voltage universal multi-mode Gm-C filter using a 180 nm TSMC technology node is presented in this paper. The proposed filter employs only three transconductance operational amplifiers (OTAs) operating in the sub-threshold region with a supply voltage of 0.5 V, resulting in a power consumption of 32 nW. Moreover, without additional active elements, the proposed circuit can operate various functional modes, such as voltage, current, transconductance, and trans-resistance. The filter's frequency, centered at 462 Hz, and a compact and low-power solution showing only 93.5 μVrms input-referred noise make the proposed filter highly suitable for bio-signal processing.

Keywords: low-power; low-voltage; Gm-C; universal filter; CMOS



Citation: Namdari, A.; Aiello, O.; Caviglia, D.D. A 0.5 V, 32 nW Compact Inverter-Based All-Filtering Response Modes Gm-C Filter for Bio-Signal Processing. *J. Low Power Electron. Appl.* **2024**, *14*, 40. <https://doi.org/10.3390/jlpea14030040>

Academic Editor: Costas Psychalinos

Received: 1 June 2024

Revised: 30 July 2024

Accepted: 1 August 2024

Published: 4 August 2024



Copyright: © 2024 by the authors. Licensee MDPI, Basel, Switzerland. This article is an open access article distributed under the terms and conditions of the Creative Commons Attribution (CC BY) license (<https://creativecommons.org/licenses/by/4.0/>).

1. Introduction

Nowadays, low-power techniques in integrated circuits (ICs) design have gained a critical role in low-power application systems. Several advanced approaches have been employed to reduce power consumption, including lowering the supply voltage, bulk-driven techniques, floating gates, and biasing transistors in the subthreshold region [1–3]. Among these, reducing the supply voltage directly reduces energy consumption, extending operation within a given power budget [3–8]. In any case, the most extreme care ought to be given to not jeopardize the proper operation of the circuit, characterized at the application level. This is particularly important for low-power bio-signal sensing devices in biomedical applications that are frequently combined with devices that gather and store energy [9–11]. However, if a high supply voltage is required, the system should be equipped with DC/DC or AC/DC converters, depending on the energy available source type [12,13]. When the converters are used in energy harvester systems, the conversion efficiency can be estimated in the range between 40% and 80%, leading to power waste [14]. As a consequence, to improve the performance and efficiency of an energy-harvested system, the use of low-power techniques will be fundamental [15–17].

From the perspective of making sensory devices, integrated filter blocks exhibit advantageous features, such as signal conditioning capabilities, and the elimination of interference and noise. One of the common filter topologies is Active-RC, which is usually used in communication systems [18]. Despite its good accuracy and low distortion, it cannot be used in applications that require low power. In analog integrated circuits, Gm-C filters are among the main building blocks, and their use has led to excellent performance, both in terms of chip size and power consumption [19–22]. An additional way to further reduce the power consumption of Gm-C filters is to implement their operational transconductance amplifiers (OTAs) by using inverter-based topologies. In fact, inverter-based OTAs offer supply voltage scalability, and thus are very effective at reducing power consumption. A range of ultra-low power analog filters with inverter-based topologies has been described in [23–25], which feature a high-frequency response and low power consumption. For different applications, analog filters with different frequency responses are required, including

low-pass (LP), high-pass (HP), band-reject (BR), all-pass (AP), and band-pass (BP). Therefore, the design of a universal filter capable of generating all possible filtering responses is often required [26,27]. There are several modes of operation for multi-mode analog filters, such as voltage mode (VM), current mode (CM), trans-resistance mode (TRM), and transconductance mode (TCM). This paper describes a low-power integrated Gm-C filter capable of generating all filtering responses under the respective operation modes.

This paper is structured as follows: Section 2 outlines the proposed filter design, while Section 3 presents the simulation results. Section 4 details the noise analysis, and Section 5 covers the sensitivity analysis. Section 6 compares the proposed filter with the state of the art. Finally, conclusions are drawn in Section 7.

2. The Proposed Filter Design

Figure 1 depicts the proposed ultra-low-power universal Gm-C filter, capable of operating in various filtering modes. i_{in1} , i_{in2} , and i_{in3} represent current inputs, while v_{in1} , v_{in2} , and v_{in3} correspond to voltage inputs. v_{OUT} denotes the output voltage, and i_{OUT} represents the output current.

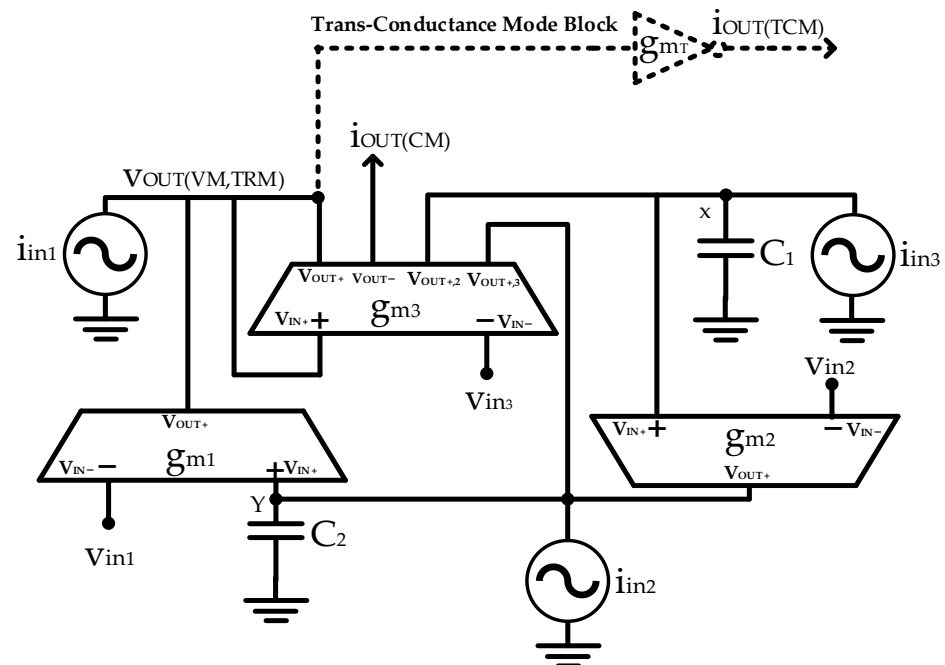


Figure 1. The proposed universal multi-mode Gm-C filter.

The proposed filter can operate in voltage, current, trans-resistance, and transconductance modes. It is composed of three gm blocks; g_{m1} , g_{m2} , and g_{m3} in Figure 1, respectively. When a transconductance mode is required, a dedicated transconductance mode block g_{mT} is added to the basic filter (dashed line in Figure 1). Furthermore, to further investigate the transfer function, Figure 2 reports the signal flow graph (SFG) of the proposed circuit. Defining $D(s)$ a polynomial function as:

$$D(s) = s^2 + \frac{g_{m1}}{C_2} s + \frac{g_{m2}g_{m1}}{C_2C_1} \tag{1}$$

The transfer functions that describe the behavior of the universal multi-mode Gm-C filter in the different operating modes are as follows:

$$v_{OUT(VM)} = \frac{D(s)v_{in3} + \frac{g_{m2}g_{m1}}{g_{m3}C_2}sv_{in2} + \frac{g_{m1}}{g_{m3}}s^2v_{in1}}{D(s)} \tag{2}$$

$$i_{OUT(TCM)} = \frac{g_{mT} \left[D(s)v_{in3} + s \frac{g_{m2}g_{m1}}{g_{m3}C_2} v_{in2} + \frac{g_{m1}}{g_{m3}} s^2 v_{in1} \right]}{D(s)} \quad (3)$$

$$i_{OUT(CM)} = \frac{s^2 i_{in1} + s \frac{g_{m1}}{C_2} i_{in2} + \frac{g_{m2}g_{m1}}{C_2C_1} i_{in3}}{D(s)} \quad (4)$$

$$v_{OUT(TRM)} = \frac{s^2 i_{in1} + s \frac{g_{m1}}{C_2} i_{in2} + \frac{g_{m2}g_{m1}}{C_2C_1} i_{in3}}{g_{m3}D(s)} \quad (5)$$

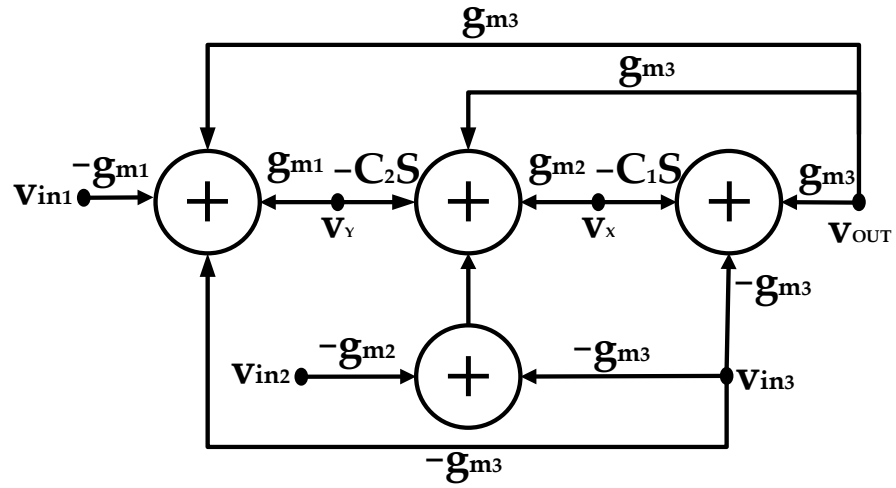


Figure 2. The signal flow graph of the Gm-C proposed filter.

2.1. Current and Trans-Resistance Modes

When $v_{in1} = v_{in2} = v_{in3} = 0$, the filter operates in the current mode, and its filtering responses are obtained as:

Low-Pass (LP): if $i_{in} = i_{in3}; i_{in1} = i_{in2} = 0$

$$\frac{i_{OUT(LP)}}{i_{in}} = \frac{g_{m2}g_{m1}}{C_2C_1} \frac{1}{D(s)}; \quad \frac{v_{OUT(LP)}}{i_{in}} = -\frac{g_{m2}g_{m1}}{g_{m3}D(s)} \quad (6)$$

High-Pass (HP): if $i_{in} = i_{in1}; i_{in2} = i_{in3} = 0$

$$\frac{i_{OUT(HP)}}{i_{in}} = \frac{s^2}{D(s)}; \quad \frac{v_{OUT(HP)}}{i_{in}} = -\frac{s^2}{g_{m3}D(s)} \quad (7)$$

Band-Pass (BP): if $i_{in} = i_{in2}; i_{in1} = i_{in3} = 0$

$$\frac{i_{OUT(BP)}}{i_{in}} = \frac{g_{m1}s}{C_2} \frac{1}{D(s)}; \quad \frac{v_{OUT(BP)}}{i_{in}} = -\frac{g_{m1}s}{g_{m3}D(s)} \quad (8)$$

Band-Reject (BR): if $i_{in} = i_{in1} = i_{in3}; i_{in2} = 0$

$$\frac{i_{OUT(BR)}}{i_{in}} = \frac{s^2 + \frac{g_{m2}g_{m1}}{C_2C_1}}{D(s)}; \quad \frac{v_{OUT(BR)}}{i_{in}} = -\frac{s^2 + \frac{g_{m2}g_{m1}}{C_2C_1}}{g_{m3}D(s)} \quad (9)$$

All-Pass (AP): if $i_{in} = i_{in1} = i_{in2} = i_{in3}$

$$\frac{i_{OUT(AP)}}{i_{in}} = \frac{s^2 + \frac{g_{m1}}{C_2}s + \frac{g_{m2}g_{m1}}{C_2C_1}}{D(s)}; \quad \frac{v_{OUT(AP)}}{i_{in}} = -\frac{s^2 + \frac{g_{m1}}{C_2}s + \frac{g_{m2}g_{m1}}{C_2C_1}}{g_{m3}D(s)} \quad (10)$$

2.2. Voltage and Transconductance Modes

When $i_{in1} = i_{in2} = i_{in3} = 0$, the voltage mode filtering responses are obtained as:

Low-Pass (LP): if $v_{in} = -v_{in1} = -v_{in2} = v_{in3}$

$$\frac{v_{OUT(LP)}}{v_{in}} = \frac{g_{m2}g_{m1}}{C_2C_1} \frac{1}{D(s)}; \quad \frac{i_{OUT(LP)}}{v_{in}} = -g_{mT} \frac{g_{m2}g_{m1}}{C_2C_1} \frac{1}{D(s)} \quad (11)$$

High-Pass (HP): if $v_{in} = v_{in1}; v_{in2} = v_{in3} = 0$

$$\frac{v_{OUT(HP)}}{v_{in}} = \frac{g_{m1}s^2}{g_{m3}} \frac{1}{D(s)}; \quad \frac{i_{OUT(HP)}}{v_{in}} = -g_{mT} \frac{g_{m1}s^2}{g_{m3}} \frac{1}{D(s)} \quad (12)$$

Band-Pass (BP): if $v_{in} = v_{in2}; v_{in1} = v_{in3} = 0$

$$\frac{v_{OUT(BP)}}{v_{in}} = \frac{g_{m2}g_{m1}s}{g_{m3}C_2} \frac{1}{D(s)}; \quad \frac{i_{OUT(BP)}}{v_{in}} = -g_{mT} \frac{g_{m2}g_{m1}s}{g_{m3}C_2} \frac{1}{D(s)} \quad (13)$$

Band-Reject (BR): if $v_{in} = -v_{in2} = v_{in3}; v_{in1} = 0$

$$\frac{v_{OUT(BR)}}{v_{in}} = \frac{s^2 + \frac{g_{m2}g_{m1}}{C_2C_1}}{D(s)}; \quad \frac{i_{OUT(BR)}}{v_{in}} = -g_{mT} \frac{s^2 + \frac{g_{m2}g_{m1}}{C_2C_1}}{D(s)} \quad (14)$$

All-Pass (AP): if $v_{in} = v_{in3}; v_{in1} = v_{in2} = 0$

$$\frac{v_{OUT(AP)}}{v_{in}} = \frac{s^2 + \frac{g_{m1}s}{C_2} + \frac{g_{m2}g_{m1}}{C_2C_1}}{D(s)}; \quad \frac{i_{OUT(AP)}}{v_{in}} = -g_{mT} \frac{s^2 + \frac{g_{m1}s}{C_2} + \frac{g_{m2}g_{m1}}{C_2C_1}}{D(s)} \quad (15)$$

Furthermore, the filter performance parameters such as the center frequency ω_0 and the quality factor Q can be calculated as:

$$\omega_0 = \sqrt{\frac{g_{m2}g_{m1}}{C_2C_1}} \quad (16)$$

$$Q = \sqrt{\frac{g_{m2}C_2}{g_{m1}C_1}} \quad (17)$$

Table 1 summarizes how different filtering functions come from a different setup of the inputs universal Gm-C filter.

Table 1. The filtering functions of the proposed universal multi-mode Gm-C filter.

Filtering Function	Input for Current and Trans-Resistance Modes	Input for Voltage and Transconductance Modes
LP	i_{in3}	$-v_{in1} = -v_{in2} = v_{in3}$
HP	i_{in1}	v_{in1}
BP	i_{in2}	v_{in2}
BR	$i_{in1} = i_{in3}$	$-v_{in2} = v_{in3}$
AP	$i_{in1} = i_{in2} = i_{in3}$	v_{in3}

3. Simulation Results

3.1. Proposed OTA and Gm-C Structures

The filter’s performance has been verified using the 180 nm TSMC technology process. The operational transconductance amplifier (OTA), which is the building block of the proposed filter, as well as the g_{mT} block required for the transconductance mode, are depicted in Figure 3a and Figure 3b, respectively. The body terminals of the NMOS transistors are tied to the ground, while the body terminals of the PMOS are usually tied to

the supply voltage V_{DD} , whether differently specified or not. In fact, the body terminals of the PMOS transistors highlighted in red in Figure 3 are connected together, and available for proper biasing. This voltage allows the center frequency of the Gm-C filter to be adjusted whenever process, supply voltage, and temperature (PVT) variations occur. The inverter-based topology can provide a transconductance gain while the circuit minimizes its power consumption. In particular, the gain of the proposed OTA is:

$$A_V = \frac{(\mathfrak{g}_{m18,21} + \mathfrak{g}_{m17,22}) \cdot (\mathfrak{g}_{m2,11} + \mathfrak{g}_{m3,12} + \mathfrak{g}_{m6,9} + \mathfrak{g}_{m7,10})}{\mathfrak{g}_{m13,14}} \cdot (r_{d18,21} \parallel r_{d16,19}) \quad (18)$$

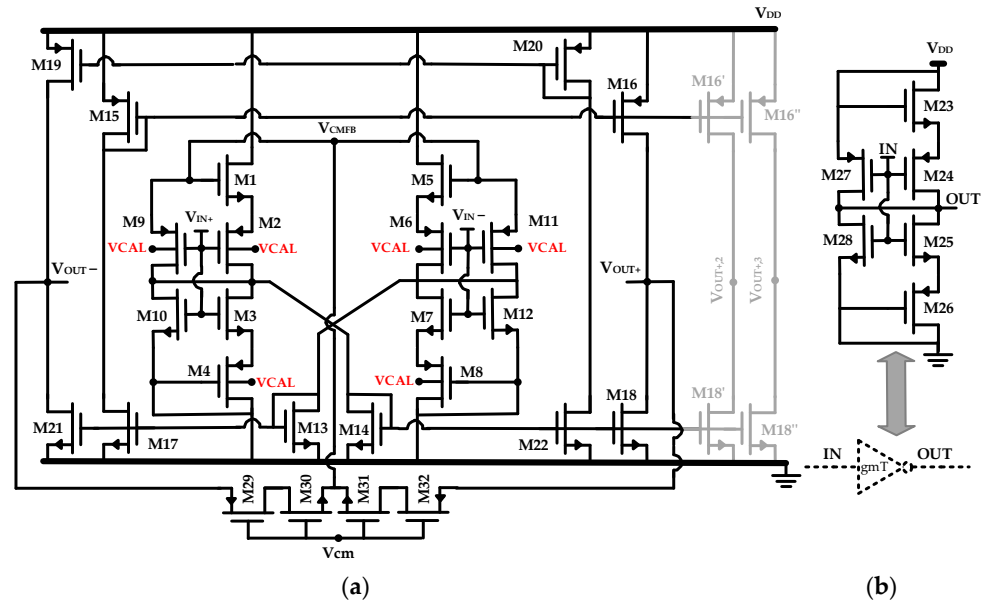


Figure 3. The circuits used in the proposed Gm-C filter (a) The proposed OTA (gray branches refer to \mathfrak{g}_{m3} block only and in red, the terminal for the calibration). (b) Transconductance mode \mathfrak{g}_{mT} block.

Table 2 summarizes the transistor aspect ratios, while Table 3 lists the features of the proposed OTA structure (Figure 3) employed in the Gm-C filter, such as DC gain, gain-bandwidth product (GBW), phase margin, CMRR, and PSRR, referring to a capacitance load value (C_L) of 1 pF. Then, the AC simulation results for the gain and phase of the proposed OTA are shown in Figure 4. Notice that two output replicas (shown in gray in Figure 3) provide additional voltages ($V_{OUT+,2}$ and $V_{OUT+,3}$) as outputs of the transconductance \mathfrak{g}_{m3} only in the proposed filter (see Figure 1). A still-inverter-based Common-mode Feedback (CMFB) circuit is made by the transistor M29-M30 and M31-M32 with a common mode voltage value of $V_{CM} = 0.3$ V (see Figure 3). The circuit exhibits an input common mode dynamic range from 0.1 V to 0.4 V.

Table 2. The aspect ratio of the OTA transistors employed in the proposed filter.

Aspect Ratio of OTA	
Transistor	W/L [$\mu\text{m}/\mu\text{m}$]
M1, M3, M5, M7, M10, M12	1/0.3 = 3.33
M2, M4, M6, M8, M9, M11	4/0.3 = 13.33
M13, M14	3/0.3 = 10
M15–M22	3/1 = 3
M29–M32	1/0.18 = 5.56
Aspect ratio of transconductance mode \mathfrak{g}_{mT} block	
Transistor	W/L [$\mu\text{m}/\mu\text{m}$]
M23, M25, M28	1/0.18 = 5.56
M24, M26, M27	4/0.18 = 22.22

Table 3. Characteristics of the proposed OTA used in the proposed filter.

Specification	Value
Supply voltage	0.5V
DC gain	46.6 dB
Phase margin	86°
GBW	17.5 kHz
CMRR	48 dB
PSRR	44 dB
Input-referred noise	503 n $\frac{V}{\sqrt{Hz}}$
Power consumption	6.3 nW
C _L	1 pF

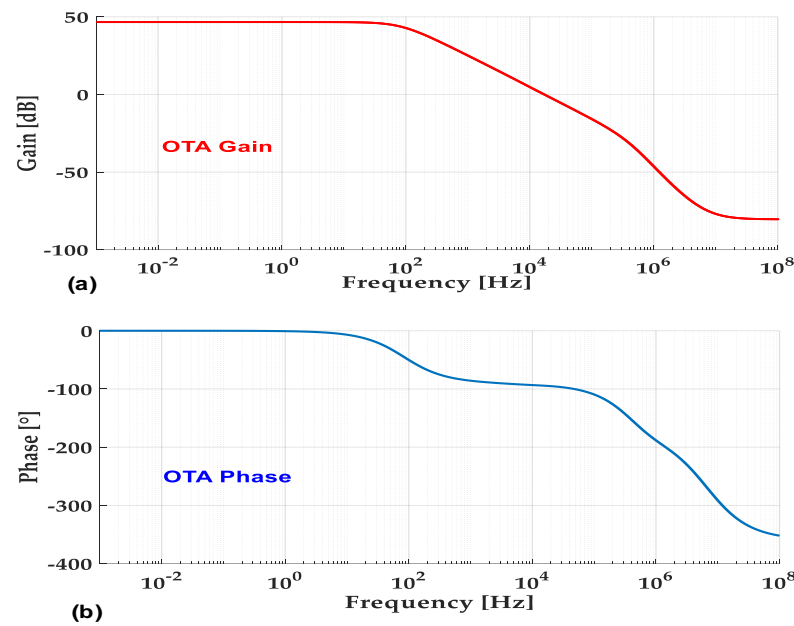


Figure 4. The OTA AC responses: (a) gain response; (b) phase response.

3.2. Gm-C Structures

Figure 5 illustrates the simulation results for the general proposed multi-mode Gm-C filter, while the transconductance (g_m) and capacitance ($C_1 = C_2$) values are 58 nS and 20 pF.

3.3. PVT Analysis

A Monte-Carlo analysis is performed to find out how process and mismatch variations affect the center frequency of the proposed Gm-C filter. Figure 6 shows the band-pass frequency response for 1000 iterations. Moreover, a complete PVT variation analysis has been performed. In particular, the center frequency of the Gm-C filter is investigated under different corner processes in Table 4. Table 5 refers to the variation in the supply voltage ($-/+10\%$), while Table 6 considers the temperature variation in a temperature range from 0 °C to 40 °C. From these tables, a significant variation in the center frequency of the proposed filter is shown. This can also be highlighted in Figures 7–9. Figure 7 depicts the band-pass frequency responses for the Gm-C filter proposed in various corners. Figures 8 and 9 illustrate the effects of supply voltage variations from 0.45 V to 0.55 V and temperature variations from 0 °C to 40 °C on the band-pass and low-pass filters, respectively.

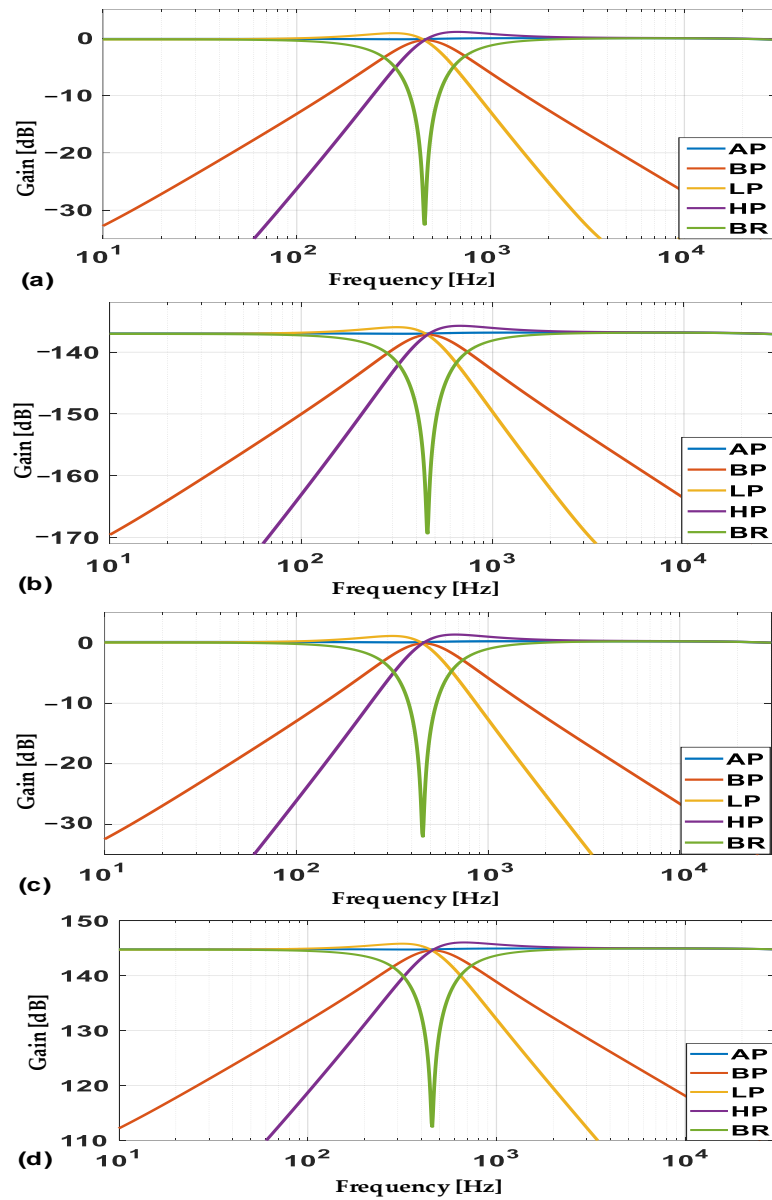


Figure 5. The frequency responses of the proposed Gm-C filter in the various modes: (a) voltage mode; (b) transconductance mode; (c) current mode; (d) trans-resistance mode.

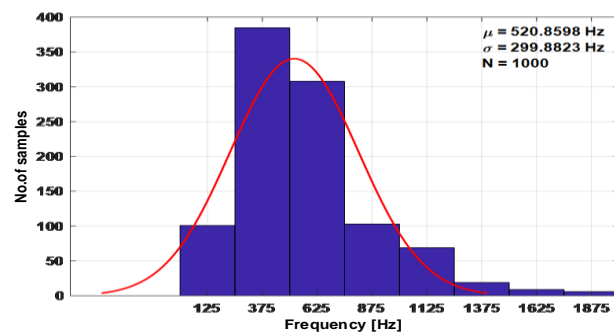


Figure 6. Monte-Carlo simulation results for the center frequency of the band-pass filter.

Table 4. The corner variations of the proposed Gm-C design.

	SS	SF	TT	FS	FF
Power consumption	8.3 nW	94.5 nW	32 nW	10 nW	118 nW
Center frequency	132 Hz	1.34 kHz	462 Hz	129 Hz	1.43 kHz

Table 5. The supply voltage variations (−/+10%) of the proposed Gm-C design.

	0.45 V	0.5 V	0.55 V
Power consumption	42 nW	32 nW	32.7 nW
Center frequency	693.4 Hz	462 Hz	305.5 Hz

Table 6. The temperature variations of the proposed Gm-C design.

	0 °C	10 °C	27 °C	40 °C
Power consumption	10 nW	16 nW	32 nW	41.5 nW
Center frequency	164.5 Hz	247 Hz	462 Hz	760 Hz

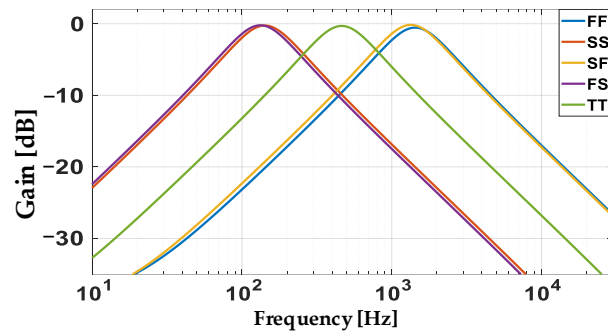


Figure 7. Variations in corner technology for the band-pass frequency response.

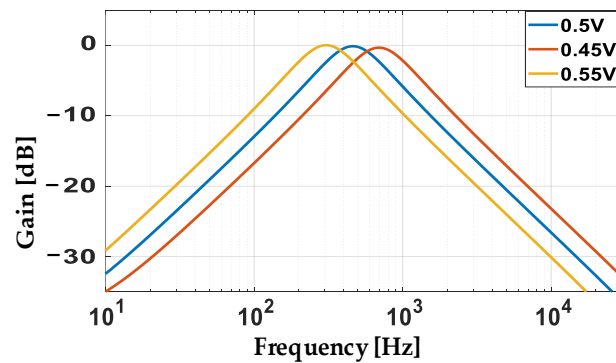


Figure 8. Variations in supply voltage for the band-pass frequency response.

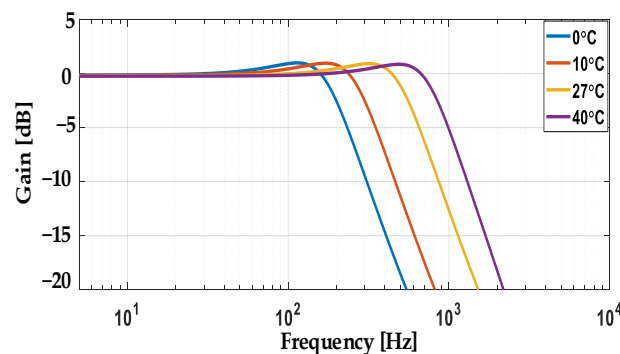


Figure 9. Variations in temperature for the low-pass frequency response.

3.4. Bulk-Biasing Technique

To compensate for the shift of the center frequency of the proposed Gm-C filter due to the PVT variations, calibration by fine-tuning the body bias of the PMOS transistors of the transconductance blocks (see V_{CAL} terminals in Figure 3) is considered. From this perspective, Table 7 shows the values of V_{CAL} to compensate for the variation in the center frequency across the five-corner process. Notice that the center frequency is affected in the corner process SS and FS and SF and FF in 132 mV and 100 mV of drift from the supply voltage allows for the re-centering of the filter on the frequency of 462 Hz. Table 8 shows how a variation of $\pm 10\%$ on the supply voltage can be compensated with only 2 mV changes of V_{CAL} . Table 9 reports how the lower temperature affected the center frequency of the filter. Thus, the circuit is suitable for integrated systems for indoor applications.

Table 7. Proposed filter’s center frequency regulation using the body-bias tuning V_{CAL} across the corner process.

	SS	SF	TT	FS	FF
Body bias of M2, M4, M6, M8, M9, M11	0.368 V	0.4 V	0.5 V	0.368 V	0.4 V
Power consumption	28.4 nW	31 nW	32 nW	32.2 nW	38 nW
Center frequency	462 Hz	462 Hz	462 Hz	462 Hz	462 Hz

Table 8. Proposed filter’s center frequency regulation using the body-bias tuning V_{CAL} for supply voltage changing $\pm 10\%$.

	0.45 V	0.5 V	0.55 V
Body bias of M2, M4, M6, M8, M9, M11	0.498 V	0.5 V	0.498 V
Power consumption	27.8 nW	32 nW	43.4 nW
Center frequency	462 Hz	462 Hz	462 Hz

Table 9. Proposed filter’s center frequency regulation using the body-bias tuning V_{CAL} at different temperatures.

	0 °C	10 °C	27 °C	40 °C
Body bias of M2, M4, M6, M8, M9, M11	0.39 V	0.43 V	0.5 V	0.45 V
Power consumption	28 nW	29.3 nW	32 nW	33 nW
Center frequency	462 Hz	462 Hz	462 Hz	462 Hz

Figure 10 shows a match between the theoretical (given by a math calculation) and simulation results for the proposed Gm-C filter. In particular, the simulation finds a frequency value of 422 Hz, while the theoretical one is $f_0 = \frac{1}{2\pi} \sqrt{\frac{g_{m2}g_{m1}}{C_2C_1}} = 426$ Hz.

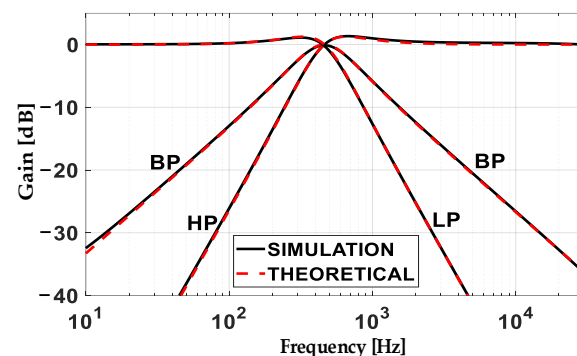


Figure 10. Comparison between simulation and theoretical results for the proposed Gm-C filter.

3.5. Group Delay of the Band-Pass Filter

The general transfer function for the band-pass filter is:

$$H(s) = \frac{\left[\frac{\omega_0}{Q}\right]s}{s^2 + \left[\frac{\omega_0}{Q}\right]s + \omega_0^2} \tag{19}$$

where ω_0 is the center pulsation and Q is the quality factor of the filter. The group delay for the band-pass filter is:

$$D(\omega) = \frac{\left[\frac{\omega_0}{Q}\right] [\omega_0^2 + \omega^2]}{[\omega_0^2 - \omega^2]^2 + \left[\frac{\omega_0}{Q}\right]^2 \omega^2} \tag{20}$$

Thus, the maximum value of the group delay for the band-pass filter is:

$$D(\omega) = \frac{2}{\left[\frac{\omega_0}{Q}\right]} = \frac{2C_2}{g_{m1}} \tag{21}$$

The group delay is shown in Figure 11: 690 μ s is the group delay at the filter’s center frequency.

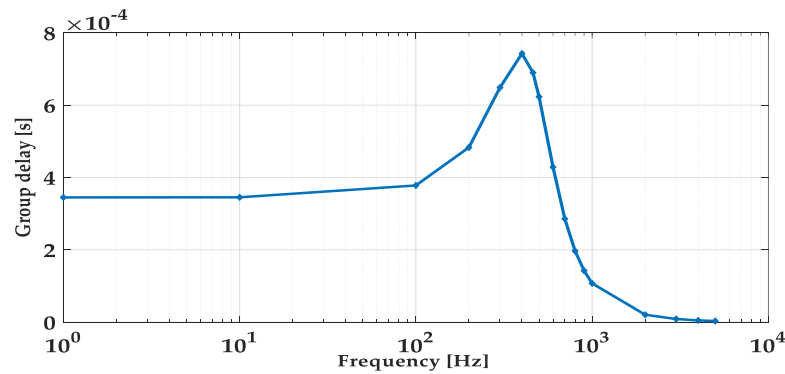


Figure 11. Group delay for the proposed band-pass filter.

3.6. The Linearity Performance of the Proposed Filter

The proposed filter’s linearity performance is investigated by applying a 40 mVPP sinusoidal input at 10 Hz. Figure 12 shows the input and output transient simulation results for different responses. Furthermore, as the input signal frequency of 10 Hz is outside the pass band of the band-pass and high-pass filters, their output signals are significantly weakened in comparison to those of the filtering responses, which are approximately the same amplitude as the input signals. Also, the input signal frequency of 462 Hz (center frequency) has been applied, as shown in Figure 13. Figure 14 highlights how the total harmonic distortion (THD) of the proposed Gm-C filter varies due to the input voltage amplitude changes between 40 mVpp and 120 mVpp. The THD values for the proposed filter for different signal amplitudes and across the five corner processes are summarized in Tables 10 and 11, respectively.

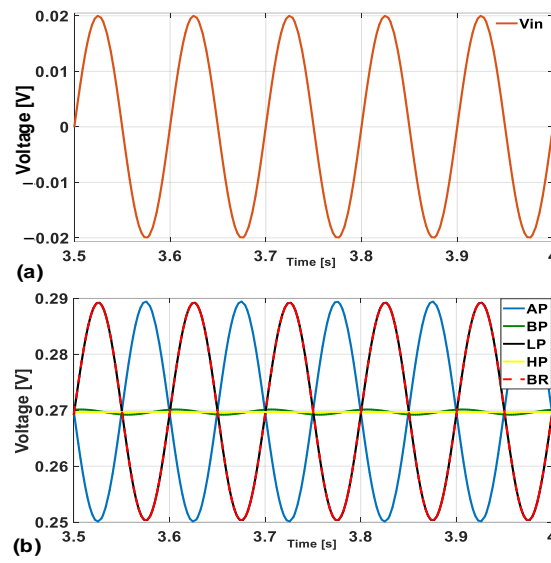


Figure 12. Transient simulation results for the proposed filter: (a) input (10 Hz); (b) output.

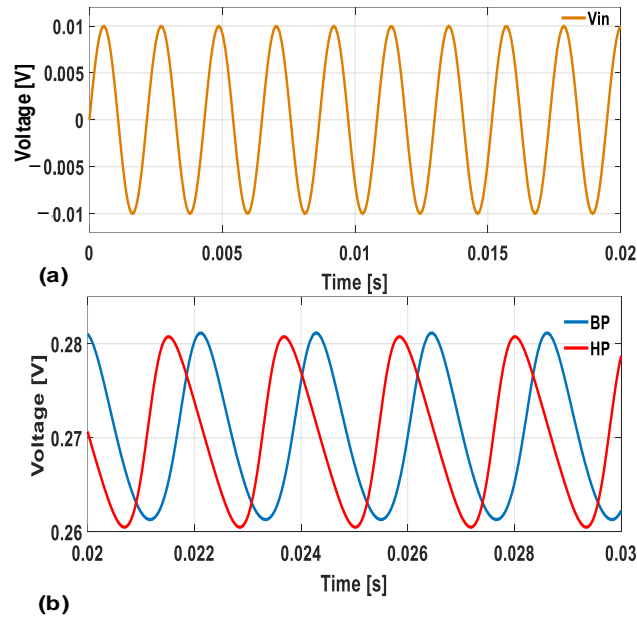


Figure 13. Transient simulation results for the proposed band-pass and high-pass filters at the center frequency (462 Hz): (a) input; (b) output.

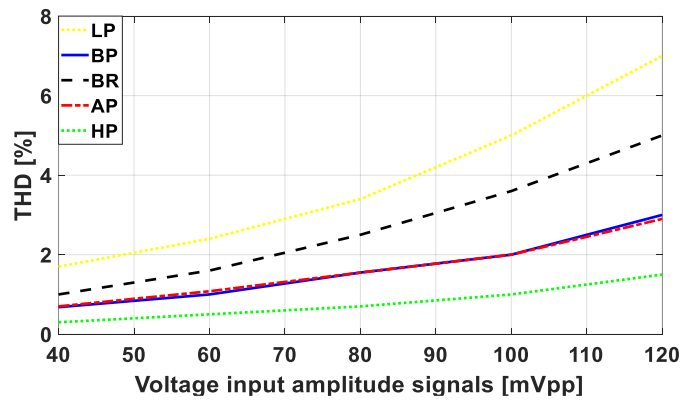


Figure 14. THD versus voltage input amplitudes.

Table 10. THD performance of the proposed filter for different signal amplitudes.

Input Voltage Amplitude (mV _{PP})	THD% at 10 Hz				
	LP	BP	BR	AP	HP
40	0.68	1	0.7	0.3	1.7
60	1	1.6	1.08	0.5	2.4
80	1.55	2.5	1.55	0.7	3.4
100	2	3.6	2	1	5
120	3	5	2.9	1.5	7

Table 11. THD performance of the proposed filter for various corner parameters.

Corner Process	THD% at 10 Hz				
	LP	BP	BR	AP	HP
SS	2.3	3.7	2.4	0.2	2.8
SF	4.8	6.6	4.8	4.7	8
FS	2	3.3	2.2	0.17	2
FF	0.5	0.3	0.48	0.47	0.94
TT	0.68	1	0.7	0.3	1.7

4. Noise Analysis

Given the low level of the input signal, the noise performance analysis is critical. To understand qualitatively how design parameters affect the overall input-referred noise, the following equations refer to the saturation region model, assumed as the worst-case scenario. In any case, the subthreshold real values are expected to be lower [28–30]. Assuming g_{mINV} , the transconductance at the OTA input terminals is as follows:

$$g_{mINV} = [g_{m2} + g_{m3} + g_{m9} + g_{m10}] \tag{22}$$

The input-referred thermal and flicker noise values for the OTA used in the proposed Gm-C filter are:

$$\overline{V_{n,Thermal}^2} = 8KT\gamma \left[\frac{g_{m14} + g_{mINV}}{g_{mINV}^2} + 2 \frac{g_{m14}^2 (g_{m16} + g_{m18})}{g_{mINV}^2 g_{m18}^2} \right] \tag{23}$$

$$\overline{V_{n,Flicker}^2} = \frac{2K_P}{C_{oxf}} \left[\frac{1}{(W \cdot L)_2} + \frac{1}{(W \cdot L)_9} \right] + \frac{2K_N}{C_{oxf}} \left[\frac{1}{(W \cdot L)_3} + \frac{1}{(W \cdot L)_{10}} + \frac{g_{m14}^2}{g_{mINV}^2 (W \cdot L)_{14}} \right] + \frac{4}{C_{oxf}} \frac{g_{m14}^2}{g_{mINV}^2} \left\{ \left[\frac{K_P}{(W \cdot L)_{16}} + \frac{K_N}{(W \cdot L)_{18}} \right] \left(1 + \frac{g_{m16}^2}{g_{m18}^2} \right) \right\} \tag{24}$$

where K is the Boltzmann constant, T is the temperature, γ is the noise factor, K_P and K_N are the flicker noise coefficients of the PMOS and NMOS transistors, C_{OX} is the gate-oxide capacitance, W is the width and L is the length of the transistors. These equations offer design guidelines for noise minimization. The overall noise is:

$$\overline{V_{n,in,OTA}^2} = \overline{V_{n,Thermal}^2} + \overline{V_{n,Flicker}^2} \tag{25}$$

Notice that g_{mINV} is roughly $4 \times$ higher than the transconductance of other transistors in the OTA topology in Figure 3. This results in the minimized input-referred noise of the overall Gm-C filter.

Considering ($|H_{N1,2,3}(s)|$) as the transfer function for each OTA input-referred noise and ($|H_B(s)|$), the band-pass filter’s transfer function is as follows:

$$|H_{N1}(s)| = \left| \frac{V_{n,OUT1}}{V_{n,in1}} \right| = \left| \frac{\frac{g_{m1} S^2}{g_{m3}}}{D(s)} \right| \tag{26}$$

$$|H_{N2}(s)| = |H_B(s)| = \left| \frac{V_{n,OUT2}}{V_{n,in2}} \right| = \left| \frac{g_{m2}g_{m1}S}{g_{m3}C_2} \right| \frac{1}{D(s)} \quad (27)$$

$$|H_{N3}(s)| = \left| \frac{V_{n,OUT3}}{V_{n,in3}} \right| = \left| \frac{s^2 + \frac{g_{m1}}{C_2}s + \frac{g_{m2}g_{m1}}{C_2C_1}}{D(s)} \right| \quad (28)$$

The input-referred noise of the three transconductance blocks for the band-pass filter ($V_{n,in,in1}$, $V_{n,in,in1}$, $V_{n,in,in3}$ in Figure 15) can be expressed by:

$$\overline{V_{n,in,in1}^2} = \left| \frac{V_{n,OUT1}}{H_B(s)} \right|^2 = \overline{V_{n,in1}^2} \left| \frac{H_{N1}(s)}{H_B(s)} \right|^2 = \overline{V_{n,in1}^2} \left[\frac{C_2S}{g_{m2}} \right]^2 \quad (29)$$

$$\overline{V_{n,in,in2}^2} = \left| \frac{V_{n,OUT2}}{H_B(s)} \right|^2 = \overline{V_{n,in2}^2} \left| \frac{H_{N2}(s)}{H_B(s)} \right|^2 = \overline{V_{n,in2}^2} \quad (30)$$

$$\overline{V_{n,in,in3}^2} = \left| \frac{V_{n,OUT3}}{H_B(s)} \right|^2 = \overline{V_{n,in3}^2} \left| \frac{H_{N3}(s)}{H_B(s)} \right|^2 = \overline{V_{n,in3}^2} \left[\frac{g_{m3}C_2D(s)}{g_{m2}g_{m1}S} \right]^2 \quad (31)$$

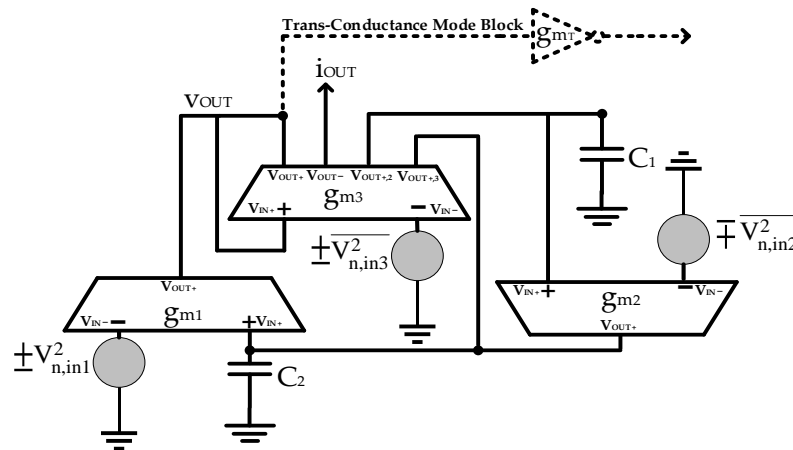


Figure 15. Modeling of the noise equivalent circuit for the proposed universal filter.

Thus, the overall equivalent input-referred noise for the band-pass filter $\overline{V_{n,in,BP}^2}$ is:

$$\overline{V_{n,in,BP}^2} = \overline{V_{n,in,in1}^2} + \overline{V_{n,in,in2}^2} + \overline{V_{n,in,in3}^2} \quad (32)$$

5. Sensitivity Analysis

Naming \check{S} the sensitivity of the K circuit characteristic with respect to the L parameter, is defined as:

$$\check{S}_L^K = \frac{\partial K}{\partial L} \cdot \frac{L}{K} \quad (33)$$

For instance, the sensitivity of the g_{m2} for the current-mode low-pass filter is calculated in (34), which is similar to the sensitivity analysis for g_{m2} in (35).

$$\check{S}_{g_{m2}}^{LPi} = \frac{\partial LP_i}{\partial g_{m2}} \cdot \frac{g_{m2}}{LP} = \frac{g_{m1}C_2C_1D(s) - g_{m2}g_{m1}^2}{D(s)^2} \cdot \frac{g_{m2}C_2C_1D(s)}{g_{m2}g_{m1}} = \frac{S^2 + \frac{g_{m1}}{C_2}S}{D(s)} \quad (34)$$

5.1. The Sensitivity Analysis of the Current-Mode Filter

The sensitivity of the universal filter responses in the current mode to the capacitance and transconductance values are as follows:

$$\check{S}_{g_{m2}}^{LP_i} = -\check{S}_{C_1}^{LP_i} = \frac{s^2 + \frac{g_{m1}}{C_2} s}{D(s)} \quad (35)$$

$$\check{S}_{C_1}^{BP_i} = -\check{S}_{g_{m2}}^{BP_i} = \frac{\frac{g_{m2} g_{m1}}{C_2 C_1}}{D(s)} \quad (36)$$

$$\check{S}_{g_{m1}}^{LP_i} = -\check{S}_{C_2}^{LP_i} = \check{S}_{g_{m1}}^{BP_i} = -\check{S}_{C_2}^{BP_i} = \frac{s^2}{D(s)} \quad (37)$$

$$\check{S}_{C_1}^{HP_i} = -\check{S}_{g_{m2}}^{HP_i} = \frac{\frac{g_{m2} g_{m1}}{C_2 C_1}}{D(s)} \quad (38)$$

$$\check{S}_{C_2}^{HP_i} = -\check{S}_{g_{m1}}^{HP_i} = \frac{\frac{g_{m1}}{C_2} s + \frac{g_{m2} g_{m1}}{C_2 C_1}}{D(s)} \quad (39)$$

$$\check{S}_{C_1}^{BP_i} = \check{S}_{C_1}^{LP_i} + \check{S}_{C_1}^{HP_i} \quad (40)$$

$$\check{S}_{C_2}^{BR_i} = \check{S}_{C_2}^{LP_i} + \check{S}_{C_2}^{HP_i} \quad (41)$$

$$\check{S}_{g_{m1}}^{BR_i} = \check{S}_{g_{m1}}^{LP_i} + \check{S}_{g_{m1}}^{HP_i} \quad (42)$$

$$\check{S}_{g_{m2}}^{BR_i} = \check{S}_{g_{m2}}^{LP_i} + \check{S}_{g_{m2}}^{HP_i} \quad (43)$$

Notice that the sum of the sensitivity values to the all-filtering responses in the current mode is zero, as reported in the following:

$$\begin{aligned} &\check{S}_{g_{m1}}^{LP_i} + \check{S}_{C_1}^{LP_i} + \check{S}_{g_{m2}}^{LP_i} + \check{S}_{C_2}^{LP_i} + \check{S}_{g_{m1}}^{BP_i} + \check{S}_{C_1}^{BP_i} + \check{S}_{g_{m2}}^{BP_i} + \check{S}_{C_2}^{BP_i} + \\ &+ \check{S}_{g_{m1}}^{HP_i} + \check{S}_{C_1}^{HP_i} + \check{S}_{g_{m2}}^{HP_i} + \check{S}_{C_2}^{HP_i} + \check{S}_{g_{m1}}^{BR_i} + \check{S}_{C_1}^{BR_i} + \check{S}_{g_{m2}}^{BR_i} + \check{S}_{C_2}^{BR_i} = 0 \end{aligned} \quad (44)$$

5.2. The Sensitivity Analysis in Voltage-Mode Filter

The sensitivity of the universal filter responses in the voltage mode to the capacitance and transconductance values are as follows:

$$\check{S}_{g_{m1}}^{LP_v} = -\check{S}_{C_2}^{LP_v} = \check{S}_{g_{m1}}^{BP_v} = -\check{S}_{C_2}^{BP_v} = \check{S}_{g_{m1}}^{HP_v} = \frac{s^2}{D(s)} \quad (45)$$

$$\check{S}_{g_{m2}}^{LP_v} = -\check{S}_{C_1}^{LP_v} = \check{S}_{g_{m2}}^{BP_v} = \frac{s^2 + \frac{g_{m1}}{C_2} s}{D(s)} \quad (46)$$

$$\check{S}_{C_1}^{BP_v} = \check{S}_{C_1}^{HP_v} = -\check{S}_{g_{m2}}^{HP_v} = \frac{\frac{g_{m2} g_{m1}}{C_2 C_1}}{D(s)} \quad (47)$$

$$\check{S}_{C_2}^{HP_v} = \frac{\frac{g_{m1}}{C_2} s + \frac{g_{m2} g_{m1}}{C_2 C_1}}{D(s)} \quad (48)$$

$$-\check{S}_{g_{m3}}^{BP_v} = -\check{S}_{g_{m3}}^{HP_v} = 1 \quad (49)$$

$$\check{S}_{C_1}^{BR_v} = \check{S}_{C_1}^{LP_v} + \check{S}_{C_1}^{HP_v} \quad (50)$$

$$\check{S}_{C_2}^{BR_v} = \check{S}_{C_2}^{LP_v} + \check{S}_{C_2}^{HP_v} \quad (51)$$

$$\check{S}_{g_{m1}}^{BR_v} = \check{S}_{g_{m1}}^{LP_v} + \check{S}_{g_{m1}}^{HP_v} \quad (52)$$

$$S_{gm2}^{BR_v} = S_{gm2}^{LP_v} + S_{gm2}^{HP_v} \tag{53}$$

Again, the sum of the sensitivity values to the all-filtering responses, also in the voltage mode, is zero:

$$S_{gm1}^{LP_v} + S_{C1}^{LP_v} + S_{gm2}^{LP_v} + S_{C2}^{LP_v} + S_{gm1}^{BP_v} + S_{C1}^{BP_v} + S_{gm2}^{BP_v} + S_{C2}^{BP_v} + S_{gm1}^{HP_v} + S_{C1}^{HP_v} + S_{gm2}^{HP_v} + S_{C2}^{HP_v} + S_{gm1}^{BR_v} + S_{C1}^{BR_v} + S_{gm2}^{BR_v} + S_{C2}^{BR_v} + S_{gm3}^{BP_v} + S_{gm3}^{HP_v} = 0 \tag{54}$$

6. Comparison with the State of the Art

Table 12 compares the proposed Gm-C circuit with the state of the art. The proposed filter shows a lower rms input-referred noise than [31–36]. Additionally, the proposed circuit consumes less power and even the figure-of-merit (FOM) for the filter. It is defined as:

$$FOM = \frac{P}{f \cdot N \cdot DR} \tag{55}$$

where P is the power consumption, f is the center frequency of the Gm-C filter, N is its order, and DR is the dynamic range.

Table 12. Gm-C filter’s state-of-the-art comparison referring to their band-pass’ central frequency.

	[31]	[32]	[33]	[34]	[35]	[36]	[37]	This Work
Supply voltage [V]	0.6	0.5	0.5	0.5	0.5	0.5	0.5	0.5
Universal	Yes	Yes	Yes	Yes	Yes	Yes	Yes	Yes
Multi-mode	Yes	Voltage	Yes	Yes	Yes	Voltage	Voltage	Yes
Filter order	2	2	2	2	2	2	2	2
Center frequency [Hz]	5000	254	211	323	114	153	10	462
Dynamic range [dB]	53.2	49.7	58.23	53.2	53.2	50	63	43.59
Rms input-refer. noise [μVrms]	155	116	130	108	208	220	45	93.5
Power consumption [μW]	5.77	0.616	0.281	0.646	0.058	0.037	0.053	0.032
FOM [10 ⁻¹² W · Hz ⁻¹ · dB ⁻¹]	1.26	3.96	0.816	2.187	0.556	2.41	1.88	0.229

7. Conclusions

An ultra-low-power, low-voltage Gm-C filter capable of producing various filtering responses (LP, HP, AP, BP, BR) in four-mode filtering operations has been designed in a 180 nm TSMC technology node. The Gm-C filter performance at a center frequency of 462 Hz has been shown in this paper. Body-bias-driven compensations for all the frequency responses under the PVT variations have also been reported. Also, the THD, the overall input-referred noise, and the sensitivity have been considered. The proposed filter operates at 0.5 V supply voltage with the minimum number of gm blocks, with its building transistors operating in the subthreshold region, showing an overall power consumption of 32 nW.

Author Contributions: Conceptualization, A.N.; methodology, A.N.; validation, A.N.; formal analysis, A.N.; investigation, A.N., O.A, and D.D.C.; resources, O.A. and D.D.C.; data curation, A.N., O.A., and D.D.C.; writing—original draft preparation, A.N.; writing—review and editing, O.A. and D.D.C.; visualization, A.N.; supervision, O.A. and D.D.C.; project administration, O.A., and D.D.C.; funding acquisition, O.A., and D.D.C. All authors have read and agreed to the published version of the manuscript.

Funding: This research received no external funding.

Data Availability Statement: Data is contained within the article.

Acknowledgments: The authors would like to thank Europractice and TSMC for PDK access.

Conflicts of Interest: The authors declare no conflict of interest.

Abbreviations

TSMC	Taiwan Semiconductor Manufacturing Company
OTA	Transconductance Operational Amplifiers
VM	Voltage Mode
CM	Current Mode
TCM	Transconductance-Mode
TRM	Trans-resistance Mode
LP	Low-Pass
HP	High-Pass
BP	Band-Pass
BR	Band-Reject
AP	All-Pass

References

- Silva, R.-S.; Rodovalho, L.-H.; Aiello, O.; Rodrigues, C.-R. A 1.9 nW, Sub-1 V, 542 pA/V linear Bulk-Driven OTA with 154 dB CMRR for Bio-Sensing Applications. *J. Low Power Electron. Appl.* **2021**, *11*, 40. [[CrossRef](#)]
- Lopez-Martin, A.; Garde, M.-P.; Algueta-Miguel, J.-M.; Beloso-Legarra, J.; Carvajal, R.-G.; Ramirez-Angulo, J. Energy-Efficient Amplifiers Based on Quasi-Floating Gate Techniques. *Appl. Sci.* **2021**, *11*, 3271. [[CrossRef](#)]
- Rodvalho, L.H.; Aiello, O.; Rodrigues, C.R. Ultra-low-voltage inverter-based Operational Transconductance Amplifiers with Voltage Gain Enhancement by Improved Composite Transistors. *Electronics* **2022**, *9*, 1410. [[CrossRef](#)]
- Garcia, J.-C.; Montiel-Nelson, J.A.; Nooshabadi, S. High Performance CMOS Level up Conversion for Systems with Low-Voltage Power Supply. In Proceedings of the IEEE International Symposium on Circuits and Systems (ISCAS), Sapporo, Japan, 26–29 May 2019; pp. 1–5.
- Rodvalho, L.-H.; Rodrigues, C.-R.; Aiello, O. Self-Biased and Supply-Voltage Scalable Inverter-Based Operational Transconductance Amplifier with Improved Composite Transistors. *Electronics* **2021**, *10*, 935. [[CrossRef](#)]
- Namdari, A.; Aiello, O.; Caviglia, D.-D. 0.5V 32nW Inverter-Based Gm-C Filter for Bio-Signal Processing. In Proceedings of the IEEE International Symposium on Circuits and Systems (ISCAS), Singapore, 19–22 May 2024; pp. 1–5. [[CrossRef](#)]
- Rodvalho, L.-H.; Aiello, O. Inverter-Based Amplifier with Active Frequency Compensation and Adaptive Voltage Scaling. In Proceedings of the IEEE International Symposium on Circuits and Systems (ISCAS), Singapore, 19–22 May 2024; pp. 1–5. [[CrossRef](#)]
- Lee, S.-Y.; Cheng, C.-J. Systematic Design and Modeling of an OTA-C Filter for Portable ECG Detection. *IEEE Trans. Biomed. Circuits Syst.* **2009**, *3*, 53–64. [[CrossRef](#)] [[PubMed](#)]
- Chen, Z.; Law, M.-K.; Mak, P.-I.; Martins, R.P. A single-chip solar energy harvesting IC using integrated photodiodes for biomedical implant applications. *IEEE Trans. Biomed. Circuits Syst.* **2017**, *11*, 44–53. [[CrossRef](#)]
- Roy, A.; Calhoun, B.H. A 71% efficient energy harvesting and power management unit for sub- μ W power biomedical applications. In Proceedings of the IEEE Biomedical Circuits and Systems Conference (BioCAS), Turin, Italy, 19–21 October 2017; pp. 1–4.
- Yi, H.; Yu, W.-H.; Mak, P.-I.; Yin, J.; Martins, R.P. A 0.18-V 382- μ W Bluetooth low-energy receiver front-end with 1.33-nW sleep power for energy-harvesting applications in 28-nm CMOS. *IEEE J. Solid-State Circuits* **2018**, *53*, 1618–1627. [[CrossRef](#)]
- Della Sala, R.; Centurelli, F.; Scotti, G.; Palumbo, G. Rail to Rail ICMR and High Performance ULV Standard-Cell-Based Comparator for Biomedical and IoT Applications. *IEEE Access* **2024**, *12*, 4642–4659. [[CrossRef](#)]
- Boragno, C.; Aiello, O.; Caviglia, D.D. Monitoring the Air Quality in an HVAC System via an Energy Harvesting Device. *Sensors* **2023**, *23*, 6381. [[CrossRef](#)]
- Sinha, A.K.; Radin, R.L.; Caviglia, D.D.; Montoro, C.G.; Schneider, M.C. An Energy Harvesting Chip designed to Extract Maximum Power from a TEG. In Proceedings of the IEEE Circuits & Systems Conference (LASCAS), Florianopolis, Brazil, 28 February–2 March 2016; pp. 1–4.
- Della Sala, R.; Centurelli, F.; Monsurrò, P.; Scotti, G.; Trifiletti, A. A 0.3V Rail-to-Rail Three-Stage OTA With High DC Gain and Improved Robustness to PVT Variations. *IEEE Access* **2023**, *11*, 19635–19644. [[CrossRef](#)]
- Toledo, P.; Aiello, O.; Crovetto, P.S. A 300mV-Supply Standard-Cell-Based OTA with Digital PWM Offset Calibration. In Proceedings of the 2019 IEEE Nordic Circuits and Systems Conference (NORCAS), Helsinki, Finland, 29–30 October 2019; pp. 1–5. [[CrossRef](#)]
- Della Sala, R.; Centurelli, F.; Scotti, G.; Tommasino, P.; Trifiletti, A. A Differential-to-Single-Ended Converter Based on Enhanced Body-Driven Current Mirrors Targeting Ultra-Low-Voltage OTAs. *Electronics* **2022**, *11*, 3838. [[CrossRef](#)]
- Ye, L.; Shi, C.; Liao, H.; Huang, R.; Wang, Y. Highly power-efficient active-RC filters with wide bandwidth-range using low-gain push-pull opamps. *IEEE Trans. Circuits Syst. I* **2013**, *60*, 95–107. [[CrossRef](#)]
- Sun, C.-Y.; Lee, S.-Y. A Fifth-Order Butterworth OTA-C LPF with Multiple-Output Differential-Input OTA for ECG Applications. *IEEE Trans. Circuits Syst. II* **2018**, *65*, 421–425. [[CrossRef](#)]
- Carrillo, J.M.; Cruz-Blas, C.A. 0.6-V 1.65- μ W Second-Order Gm-C Bandpass Filter for Multi-Frequency Bioimpedance Analysis Based on a Bootstrapped Bulk-Driven Voltage Buffer. *J. Low Power Electron. Appl.* **2022**, *12*, 62. [[CrossRef](#)]

21. Sala, R.-D.; Monsurrò, P.; Scotti, G.; Trifiletti, A. Area-Efficient Low-Power Bandpass Gm-C Filter for Epileptic Seizure Detection in 130nm CMOS. In Proceedings of the IEEE Int. Electronics, Circuits and Systems Conference (ICECS), Genoa, Italy, 27–29 November 2019; pp. 1–4.
22. Della Sala, R.; Centurelli, F.; Scotti, G. A Novel High Performance Standard-Cell Based ULV OTA Exploiting an Improved Basic Amplifier. *IEEE Access* **2024**, *12*, 17513–17521. [[CrossRef](#)]
23. Ramesh, N.; Gaggatur, J.-S. A 0.6 V, 2nd order low-pass Gm-C filter using CMOS inverter-based tunable OTA with 1.114 GHz cut-off frequency in 90 nm CMOS technology. In Proceedings of the 2021 34th International Conference on VLSI Design and 2021 20th International Conference on Embedded Systems (VLSID), Guwahati, India, 20–24 February 2021; pp. 305–309.
24. Deng, J.; Fu, Z.; Wang, Z.; Chen, D.; Tang, X.; Guo, J. Improved Nauta Transconductor for Wideband Intermediate-Frequency gm-C Filter. In Proceedings of the IEEE International Symposium on Circuits and Systems (ISCAS), Baltimore, MD, USA, 28–31 May 2017; pp. 1–4.
25. Kweon, S.-J.; Shin, S.-H.; Jo, S.-H.; Yoo, H.-J. Reconfigurable High-Order Moving-Average Filter Using Inverter-Based Variable Transconductance Amplifiers. *IEEE Trans. Circuits Syst. II* **2014**, *61*, 942–946. [[CrossRef](#)]
26. Jaikla, W.; Khateb, F.; Kulej, T.; Pitaksuttayaprot, K. Universal Filter Based on Compact CMOS Structure of VDDDA. *Sensors* **2021**, *21*, 1683. [[CrossRef](#)] [[PubMed](#)]
27. Kumngern, M.; Khateb, F.; Kulej, T.; Psychalions, C. Multiple-Input Universal Filter and Quadrature Oscillator Using Multiple-Input Operational Transconductance Amplifiers. *IEEE Access* **2021**, *9*, 56253–56263. [[CrossRef](#)]
28. Binkley, D.M. *Tradeoffs and Optimization in Analog CMOS Design*; John Wiley & Sons: Hoboken, NJ, USA, 2008. [[CrossRef](#)]
29. Chang, J.; Abidi, A.A.; Viswanathan, C.R. Flicker noise in CMOS transistors from subthreshold to strong inversion at various temperatures. *IEEE Trans. Electron Devices* **1994**, *41*, 1965–1971. [[CrossRef](#)]
30. Allogo, Y.A.; Marin, M.; de Murcia, M.; Llinares, P.; Cottin, D. 1/f noise in 0.18 μm technology n-MOSFETs from subthreshold to saturation. *Solid-State Electron.* **2002**, *46*, 977–983. [[CrossRef](#)]
31. Namdari, A.; Dolatshahi, M. Design of a low-voltage and low-power, reconfigurable universal OTA-C filter. *Analog. Integr. Circuits Signal Process.* **2022**, *111*, 169–188. [[CrossRef](#)]
32. Khateb, F.; Kumngern, M.; Kulej, T.; Biolk, D. 0.5 V Differential Difference Transconductance Amplifier and Its Application in Voltage-Mode Universal Filter. *IEEE Access* **2022**, *10*, 43209–43220. [[CrossRef](#)]
33. Khateb, F.; Kumngern, M.; Kulej, T. 0.5-V 281-nW Versatile Mixed-Mode Filter Using Multiple-Input/Output Differential Difference Transconductance Amplifiers. *Sensors* **2023**, *24*, 32. [[CrossRef](#)] [[PubMed](#)]
34. Kulej, T.; Kumngern, M.; Khateb, F.; Arbet, D. 0.5 V Versatile Voltage- and Transconductance-Mode Analog Filter Using Differential Difference Transconductance Amplifier. *Sensors* **2023**, *23*, 688. [[CrossRef](#)] [[PubMed](#)]
35. Khateb, F.; Kumngern, M.; Kulej, T. 58-nW 0.5-V mixed-mode universal filter using multiple-input multiple-output OTAs. *IEEE Access* **2023**, *11*, 130345–130357. [[CrossRef](#)]
36. Khateb, F.; Kumngern, M.; Kulej, T.; Akbari, M.; Stopjakova, V. 0.5 V, nW-Range Universal Filter Based on Multiple-Input Transconductor for Biosignals Processing. *Sensors* **2022**, *22*, 8619. [[CrossRef](#)]
37. Jaikla, W.; Khateb, F.; Kumngern, M.; Kulej, T.; Ranjan, R.-K.; Suwanjan, P. 0.5 V Fully Differential Universal Filter Based on Multiple Input OTAs. *IEEE Access* **2020**, *8*, 187832–187839. [[CrossRef](#)]

Disclaimer/Publisher’s Note: The statements, opinions and data contained in all publications are solely those of the individual author(s) and contributor(s) and not of MDPI and/or the editor(s). MDPI and/or the editor(s) disclaim responsibility for any injury to people or property resulting from any ideas, methods, instructions or products referred to in the content.